IVYSPRING INTERNATIONAL PUBLISHER

Theranostics

2019; 9(1): 179-195. doi: 10.7150/thno.29545

Research Paper

OTUB2 stabilizes U2AF2 to promote the Warburg effect and tumorigenesis via the AKT/mTOR signaling pathway in non-small cell lung cancer

Jing Li[1*], Dongdong Cheng[2*], Miaoxin Zhu[1], Huajian Yu[1], Zhen Pan[2], Lei Liu[1], Qin Geng[1], Hongyu Pan[1], Mingxia Yan[1✉], Ming Yao[1✉]

1. State Key Laboratory of Oncogenes and Related Genes, Shanghai Cancer Institute, Renji Hospital, Shanghai Jiao Tong University School of Medicine, Shanghai, China
2. Department of Orthopedics, Shanghai Jiao Tong University Affiliated Sixth People's Hospital, Shanghai, China

* These authors contributed equally to this work.

✉ Corresponding author: State Key Laboratory of Oncogenes and Related Genes, Shanghai Cancer Institute, Renji Hospital, Shanghai Jiao Tong University School of Medicine, No. 25/2200, Xietu Road, Shanghai 200032, China. Tel: +86 2164183618; Fax: +86 21 64042002. Email: myao@shsci.org; mxyan@shsci.org

Received: 2018.08.28; Accepted: 2018.11.25; Published: 2019.01.01

Abstract

Increasing evidence has confirmed that deubiquitinating enzymes play an important role in lung cancer progression. In the current study, we investigated the expression profile of deubiquitinating enzymes in non-small cell lung cancer (NSCLC) tissues and identified OTUB2 as an upregulated deubiquitinating enzyme. The role of OTUB2 in NSCLC is unknown.

Methods: Quantitative, real-time PCR and Western blot were used to detect OTUB2 and U2AF2 expression in NSCLC tissues. The correlations between OTUB2 and U2AF2 expression and clinicopathologic features were then analyzed. We used *In vitro* Cell Counting Kit-8 (CCK-8) , colony formation , and trans-well invasion assays to investigate the function of OTUB2 and U2AF2 in tumorigenesis. The regulation of glycolysis by OTUB2 and U2AF2 was assessed by determining the extracellular acid ratio, glucose consumption, and lactate production. The mechanism of OTUB2 was explored through co-immunoprecipitation and mass spectrometry analyses. A xenograft model was also used to study the tumorigenesis role of OTUB2 *In vivo*.

Results: OTUB2 expression was significantly upregulated in primary NSCLC tissues and greatly associated with metastasis, advanced tumor stages, poor survival, and recurrence. In NSCLC cell lines, OTUB2 promoted cell growth, colony formation, migration, and invasive activities. Mechanistic investigations showed that OTUB2 stimulated the Warburg effect and induced the activation of the serine/threonine kinase/mechanistic target of rapamycin kinase (AKT/mTOR) pathway in different NSCLC cells. More importantly, OTUB2 promoted NSCLC progression, which was largely dependent on the direct binding to and deubiquitination of U2AF2, at least in NSCLC cells. U2AF2 expression was also significantly upregulated in primary NSCLC tissues and dramatically associated with metastasis, advanced tumor stages, poor survival, and recurrence. Importantly, a positive correlation between the protein expression of OTUB2 and U2AF2 in NSCLC tissues was found. *In vivo* experiments indicated that OTUB2 promoted xenograft tumor growth of NSCLC cell. In addition, our results suggest that high expression of OTUB2, U2AF2 and PGK1 is significantly associated with worse prognosis in NSCLC patients.

Conclusion: Taken together, the present study provides the first evidence that OTUB2 acts as a pivotal driver in NSCLC tumorigenesis by stabilizing U2AF2 and activating the AKT/mTOR pathway and the Warburg effect. It may serve as a new potential prognostic indicator and therapeutic target in NSCLC.

Key words: deubiquitinating enzyme, OTUB2, NSCLC, Warburg effect, U2AF2

Introduction

Lung cancer is the second most commonly diagnosed cancer after prostate cancer in men and breast cancer in women worldwide [1]. It is the leading cause (25%) of all cancer deaths, exceeding those of any other type of cancer in both men and women worldwide. Non-small cell lung cancer (NSCLC) accounts for approximately 85% histological types of lung cancer and mainly includes adenocarcinoma (AD) and squamous cell carcinoma (SCC) [2]. In contrast to the steady increase in survival observed for most cancer types, the 5-year relative survival rate of lung cancer advances slowly, remaining only at 18% [3]. Over the past decades, approximately 90% of patients diagnosed with NSCLC have died due to distant metastases rather than the primary tumor. Distant metastases are also primarily responsible for the failure of lung cancer prognosis and therapy [4, 5]. However, the mechanisms involved in lung cancer remain unclear.

Protein post-translational modifications play vital roles in controlling the activity, interactions, subcellular location and stability of many proteins. The ubiquitin-proteasome system (UPS) is the main pathway of protein post-translational modifications and is mediated by E1, E2, and E3 ubiquitin ligases and deubiquitinating enzymes (DUBs). Protein ubiquitination-mediated degradation is a reversible process in which ubiquitin conjugation is mediated via the sequential activity of E1 ubiquitin-activating enzymes, E2 ubiquitin-conjugating enzymes, and E3 ubiquitin ligases and catalyzes the ubiquitination of proteins to target them for proteasomal degradation. Ubiquitin removal from poly-ubiquitin chains is catalyzed by DUBs [6-8]. The human genome encodes at least 98 DUBs which are classified into 6 families based on sequence and structural similarity: ubiquitin carboxyl-terminal hydrolases (UCHs), ubiquitin-specific proteases (USPs), ovarian tumor-like proteases (OTUs), Josephins and JAB1/MPN/MOV34 metalloenzymes (JAMMs), and motif interacting with ubiquitin-containing novel DUB family (MINDYs) [9]. A number of recent studies have revealed that the wide functional diversity of DUBs has a profound impact on the regulation of multiple biological processes, such as cell cycle regulation, DNA repair, chromatin remodeling and several signaling pathways that are frequently altered in cancer. Several DUBs, including USP16, USP3, USP22, and USP48, have been implicated in histone deubiquitination [10-12], while USP1, USP13, USP9X, and zinc finger containing ubiquitin peptidase 1 (ZUP1) have been implicated in the DNA damage response [13-16]. CYLD lysine 63 deubiquitinase (CYLD) and TNF alpha induced protein 3 (TNFAIP3) negatively regulate the nuclear factor kappa B (NF-κB) pathway; OTUD3 regulates phosphatase and tensin homolog (PTEN) stability and suppresses tumorigenesis; and OTU deubiquitinase 7B (OTUD7B) regulates mechanistic target of rapamycin kinase C2 (mTORC2) signaling pathways [17-19]. Although a large number of DUBs have recently been implicated in various tumorigenic progresses, the functions of DUBs in NSCLC are poorly understood. The limited understanding of the biological functions of DUBs in NSCLC led us to perform a dysregulated DUBs genes analysis in 83 paired NSCLC samples and adjacent noncancerous lung tissues (Gene Expression Omnibus [GEO] Submission: GSE75037) and identify oncogenic or tumor suppressor DUBs, thereby aiding in the elucidation of the biological functions of DUBs in NSCLC.

In our study, OTUB2 was upregulated in lung cancer tissues and negatively associated with poor patient prognosis. OTUB2, described as a deubiquitylating enzyme, belongs to the ovarian tumor (OTU) superfamily of proteins that was first identified in an ovarian tumor gene from *Drosophila melanogaster* [20]. OTUB2 has a wide range of biological roles, including protecting against virus-induced activation of interferon regulatory factor 3 (IRF3) and NF-κB [21], promoting beta cell survival in human pancreatic islets [22], and supporting the DNA repair pathway [23, 24]. However, our knowledge of the function of OTUB2 in tumor development is limited. Here, we demonstrate, for the first time, that OTUB2 acts as a novel promoter of NSCLC by stabilizing U2 small nuclear ribonucleoprotein auxiliary factor 2 (U2AF2). It also activates the AKT/mTOR pathway and the Warburg effect and may serve as a new potential prognostic indicator and therapeutic target in NSCLC.

Methods

Cell culture

Eight human NSCLC cell lines (PC-9, H1975, H838, A549, H1299, H292, H460, and 293T) were obtained from the American Tissue Culture Collection (ATCC) (Manassas, VA, USA). All cell lines were cultured according to ATCC protocols and supplemented with 10% fetal bovine serum (FBS) (Biowest, South America Origin, Nuaille, France), 100 U/mL penicillin sodium, and 100 μg/mL streptomycin sulfate at 37 °C in a humidified incubator under 5% carbon dioxide. XL-2 and LC-21 cells were established by our laboratory [25, 26]. Cells were used when they were in the logarithmic growth phase. These cell lines were mycoplasma-free and

authenticated by quality examinations of morphology and growth profile.

Human NSCLC samples

Seventy-three paired human NSCLC samples and their matched adjacent non-cancerous tissues from patients who had undergone surgery were obtained from the Department of Lung Cancer, Shanghai Chest Hospital, from 2011 to 2012. Human surgical tissues were immediately frozen in liquid nitrogen and stored at -80 °C refrigerator. The patients had not received chemotherapy, radiotherapy, hormone therapy or other related anti-tumor therapies before surgery. Institutional review board approval and written informed consent from each patient were obtained.

RNA extraction and real-time polymerase chain reaction assay

Total RNA samples were isolated from the NSCLC tissue specimens and cell lines in this study with TRIzol reagent (Invitrogen, California, USA) according to the manufacturer's protocol. cDNA synthesis was subsequently performed by the PrimeScript RT Reagent Kit (TaKaRa, Dalian, China) according to the manufacturer's protocol. Real-time polymerase chain reaction (qPCR) was performed using SYBR Green Premix Ex Taq (TaKaRa, Dalian, China) according to the manufacturer's protocol. See **Table S1** for the primers used. β-actin was used as the internal control.

Western blot

All protein samples were isolated from the NSCLC tissue specimens and cell lines in this study using Tissue Protein Extraction Reagent (Thermo Fisher, Waltham, USA) with a cocktail of proteinase inhibitors and phosphatase inhibitors (Roche Applied Science, Indianapolis, USA). Protein concentration was measured by the bicinchoninic acid (BCA) Protein Assay Kit (Thermo Fisher, Waltham, USA). Protein lysates were separated by SDS-PAGE gel electrophoresis and transferred to Polyvinylidene Fluoride (PVDF) membrane (Millipore, Massachusetts, USA). After blocking with 5% skimmed milk, the membrane was probed with the primary antibodies and species-specific secondary antibodies. See **Table S2** for the antibodies used**siRNAs.**

siRNA oligonucleotides targeting *OTUB2* and *U2AF2* were designed and synthesized by RiboBio (Guangzhou, China). Cells were plated at 60-70% confluence in a 6-well plate and transfected with a scrambled siRNA or the indicated siRNA using Lipofectamine 2000 Reagent (Invitrogen, California, USA) according to the manufacturer's protocol. All siRNA oligonucleotides used are listed in **Table S1**.

Lentivirus constructs

Hemagglutinin-OTUB2 (HA-OTUB2) (ID: 78990), OTUB2 mutant (HA-OTUB2^{C51S}) with the depletion of carboxyl terminal (51–62aa), as well as Flag-U2AF2 (ID: 11338) were cloned into the lentiviral expression vector pWPXL. The plasmids expressing V5-ubiquitin were kindly provided by Dr Fanglin Zhang. Primers for PCR were designed to include BamHI and XhoI restriction sites. For virus production, 12 μg of the HA-OTUB2, HA-OTUB2^{C51S} and Flag-U2AF2 plasmid, 9 μg of the packaging plasmid psPAX2 and 3.6 μg of the envelope plasmid pMD2.G were transfected into 293T cells cultured at 80% confluence in a 100-mm dish using Lipofectamine 2000 (Invitrogen, California, USA) according to the manufacturer's instructions. Viruses were harvested 48 h after transfection and filtered through a 0.45-mm filter. Cells (1×10^5), including XL-2, H292 and 293T, were infected with 1×10^6 recombinant lentivirus-transducing units in the presence of 6 μg/mL polybrene (Sigma-Aldrich, Saint Louis, Missouri, USA).

Cell proliferation, migration and invasion assays

In vitro proliferation of A549, H1299, XL-2, and H292 were measured using Cell Counting Kit-8 (CCK-8) (Dojindo, Kumamoto, Japan). According to the manufacturer's instructions, all the cells were plated in triplicates in 96-well plates at 1.0×10^3 cells per well in a 200-μL volume. Cell migration and invasion assays were performed by Transwell filter chambers (BD Biosciences, New Jersey, USA). For migration assays, 5×10^4 A549 and H1299 cells or 1×10^5 XL-2 and H292 cells in a 200-μL,serum-free culture medium were suspended into the upper chamber per well. For invasion assays, 1×10^5 A549 and H1299 cells or 2×10^5 XL-2 and H292 cells in a 200-μL,serum-free culture medium were placed into the upper chamber per well with a Matrigel-coated membrane diluted with serum-free culture medium. An 800-μL culture medium supplemented with 10% FBS was added in the lower chamber. After incubation at 37 °C in a humidified incubator under 5% carbon dioxide , the cells in the bottom surface of the membrane were fixed with 100% methanol, stained with 0.1% crystal violet for 30 min, and counted under a light microscope.

Wound-healing assays

For cell motility assay, all the lung cancer cell lines were seeded in six-well plates to reach 90% confluence. A single scratch wound was created using a 200-μL pipette tip, and the cell debris was removed

by washing with PBS and replaced with culture medium (1% FBS). The images were immediately photographed at 0 h, 24 h or 48 h after wounding. The wound sizes were measured by Magnetic Resonance Imaging (MRI) Wound Healing Tool in Image J.

ECAR and OCR

The Seahorse XF96 Flux Analyzer (Seahorse Bioscience, Billerica, Massachusetts, USA) was used to measure the oxygen consumption rate (OCR) and extracellular acidification rate (ECAR) in lung cancer cells according to the manufacturer's instructions. Approximately 1×10^5 A549, H1299, XL-2, and H292 cells per well were seeded into an XF96-well plate and attached overnight. For the assessment of ECAR, cells were incubated with non-buffered RPMI 1640 under basal conditions followed by a sequential injection of 10 mM glucose, 1 mM mitochondrial poison (oligomycin, Sigma-Aldrich, Saint Louis, Missouri, USA) and 80 mM glycolysis inhibitor (2-deoxyglucose, 2-DG, Sigma-Aldrich). OCR was assessed under basal conditions and after sequential injection of 1 μM oligomycin, 1 μM fluoro-carbonyl cyanide phenylhydrazone (FCCP) and 2 mM antimycin A and rotenone (Sigma-Aldrich, Saint Louis, Missouri, USA). Both ECAR and OCR measurements were normalized to total protein content.

Measurement of glucose and lactate

Glucose consumption was measured using a glucose assay kit (Sigma-Aldrich, Saint Louis, Missouri, USA) according to the manufacturer's instructions. NSCLC cells were seeded into a 6-well plate. The culture medium was collected to measure glucose and lactate concentrations, and cells were harvested to obtain protein lysates. For the glucose consumption of NSCLC cells, the following solutions were pipetted into the appropriately marked test tube: reagent blank (1 mL water), standard (0.95 mL water + 0.05 mL glucose standard), and test (1 mL sample). At time zero, the reaction was started by adding 2 mL of assay reagent to the first tube and mixing. A 30-60 s interval was allowed between additions of the assay reagent to each subsequent tube. Each tube was allowed to react for exactly 30 min at 37 °C. The reaction was stopped at 30–60 s intervals by adding 2 mL of 12 N H_2SO_4 into each tube. Each tube was carefully mixed. The absorbance of each tube was measured against the reagent blank at 540 nm. Glucose consumption was calculated by deducting the measured glucose concentration in the medium from the original glucose concentration. Lactate production was determined by using the Lactate Assay Kit (Sigma-Aldrich, Saint Louis, Missouri, USA) according to the manufacturer's instructions. Briefly, 50 μL of the master reaction mix (46 μL lactate assay buffer + 2 μL lactate enzyme mix + 2 μL lactate probe) was added to each well. The reaction was mixed well by pipetting and incubating for 30 min at room temperature. The plate was protected from light during the incubation. For colorimetric assays, the absorbance at 570 nm (A570) was measured. The results were normalized to the total protein concentration of each sample. All experiments were performed in triplicate and repeated three times.

Co-immunoprecipitation and mass spectrometry

Cells were harvested using immunoprecipitation (IP) lysis buffer (Beyotime Institute of Biotechnology, Shanghai, China) with a cocktail of proteinase inhibitors (Roche Applied Science, Switzerland). Total protein (up to 3 mg) was incubated with 30 μL of protein A/G immunoprecipitate magnetic beads (Millipore, Massachusetts, USA) to reduce non-specific binding for 2 h. The beads were removed and 12 μL of the primary antibody (OTUB2, U2AF2) or isotype IgG was added to the supernatant at 4 °C on a rocking platform overnight. A total of 40 μL of protein A/G beads was then added to each immunoprecipitation mixture for 4 h. The immunoprecipitates were collected by a magnetic separator and washed three times with the cooled IP lysis buffer. The lysis buffer was subsequently removed. Then, 40 μL of 2 × loading buffer was added to the agarose, boiled for 10 min and subjected to Western blot analysis. EasyBlot anti-rabbit (GTX221666-01) IgG (GeneTex, California, USA), which is a horseradish peroxidase (HRP)-conjugated secondary antibody, were employed to avoid the interference from heavy and light chains of antibodies in IP assays. Hemagglutinin (HA) Affinity Gel (Sigma-Aldrich, Saint Louis, Missouri, USA, A2220) was used to immunoprecipitate HA-tagged proteins. Bound proteins were separated by SDS-PAGE and stained with the Silver Staining Kit (Beyotime Biotechnology, Shanghai, China). The specific bands were identified and the peptides were digested with trypsin. The peptides were then analyzed on an Orbitrap Fusion mass spectrometer (Thermo Fisher, Waltham, USA). Protein identification was performed by ProteinPilot 4.1 (AB Sciex, Texas, USA).

In vitro deubiquitination assay

Ub-V5 conjugated U2AF2-Flag was purified from HEK293T cells with anti-Flag M2 Affinity Gel (Sigma-Aldrich, Saint Louis, Missouri, USA). The protein complexes containing HA tagged wild-type OTUB2 or the C51S mutant type of OTUB2 were

purified from HEK293T cells with anti-HA Affinity Gel (Sigma-Alrich). UB-HA-U2AF2 and the OTUB2 protein complexes were incubated for 1 h at 37 °C in the reaction buffer (50 mM Tris pH 7.5, 10 mM $MgCl_2$, 1 mM DTT, 100 mM NaCl, 1 mM ATP). After the reaction, the U2AF2-Flag protein was purified and immunoblotted with antibodies against V5.

Xenograft model

Five-week-old BALB/c-nu/nu nude male mice were used for our animal studies, and all animals were maintained in specific-pathogen-free (SPF) conditions. The mice were subcutaneously injected with 3×10^6 XL-2 cells which had been infected with virus expressing either stable OTUB2 overexpression or empty vector (8 per group). Tumor volumes were measured at the indicated time intervals. The tumor-bearing mice were sacrificed 24 days after inoculation, and the tumors were removed for further study. Tumor volume was calculated as follows: V (volume) = (length × width^2)/2. All experiments were subject to approval by the Animal Care and Use Committee of Shanghai Cancer Institute.

Statistical analysis

The data were compiled and analyzed using SPSS 16.0 (IBM, New York, USA). Two-tailed Student's t-test and one-way ANOVA were used for comparisons between two groups and between more than two groups, respectively. Survival curves were calculated using the Kaplan–Meier method and analyzed by the log-rank test. Correlations of OTUB2 and U2AF2 expression with categorical, clinical variables in NSCLC were evaluated using the Fisher's exact test. Correlations between OTUB2 and U2AF2 were analyzed using the Spearman's correlation test. Values of $P < 0.05$ were considered statistically significant. Data are presented as the mean ± SEM from one representative experiment of three independent experiments, and every representative experiment was repeated three times.

Results

OTUB2 is upregulated in NSCLC and is associated with patient prognosis

To identify the deubiquitinating enzymes driving NSCLC progression, we compared dysregulated genes in 83 paired NSCLC samples with adjacent noncancerous lung tissues (GEO Submission: GSE75037) and detected five upregulated deubiquitinating enzymes (USP49, JOSD2, OTUB1, USP48 and OTUB2) in lung cancer tissues (**Figure 1A** and **Figure S1A**). Next, Kaplan-Meier's survival analysis was performed to examine the expression of five deubiquitinating enzymes in 117 NSCLC patients (GEO Submission: GSE13213) and revealed that the higher expression of OTUB1 and OTUB2 was significantly associated with poor patient prognosis (**Figure S1B-E** and **Figure 1E**). OTUB1 promotes cancer cell invasion and tumorigenesis in various human cancers [27-30], while the role of OTUB2 in cancer progression remains unknown.

To assess the underlying role of OTUB2 in NSCLC, we analyzed OTUB2 mRNA expression in 73 paired NSCLC samples and adjacent noncancerous lung tissues by real-time PCR. OTUB2 expression was significantly increased in clinical NSCLC samples compared to their corresponding noncancerous lung tissues (**Figure 1B** and **Table 1**). Clinical association studies found that OTUB2 expression was significantly associated with lymph node and distal metastasis (P=0.0330) as well as advanced tumor node metastases (TNM) stages (P=0.0335) (**Figure 1C-D** and **Table 1**). By comparing OTUB2 expression between NSCLC patients with and without relapse, we found that OTUB2 was increased in relapsed patients (**Figure 1F**). In addition, the TIMER database (http://cistrome.org/timer) showed that OTUB2 was upregulated in various human cancers (**Figure S1F**). Taken together, these findings suggest that OTUB2 could serve as an effective predictor of malignant progression in NSCLC.

Table 1. Correlation between OTUB2 levels in NSCLC patients and their clinicopathologic characteristics.

Clinicopathologic parameters	Number of cases	Median expression of OTUB2	
		Mean±SD	*P*-value
Age (year)			
≤60	31	0.00010 ± 0.00002	0.8423
>60	42	0.00010 ± 0.00002	
Gender			
Male	44	0.00011 ± 0.00002	0.2593
Female	29	0.00007 ± 0.00002	
Tumor size(cm)			
≤3	28	0.00007 ± 0.00002	0.1448
>3	45	0.00012 ± 0.00002	
TNM stage			
Stage I + II	35	0.00007 ± 0.00001	0.0335*
Stage III+IV	38	0.00016 ±0.00002	
Metastasis			
No	35	0.00007 ± 0.00002	0.0330*
Yes	38	0.00013 ± 0.00003	
Carcinoma			
NSCLC	73	0.00003 ± 0.00005	< 0.0001***
Adjacent Lung	73	0.00010 ± 0.00002	
Pathologic classification			
Adenocarcinoma	57	0.00010 ± 0.00002	0.9754
Squamous carcinoma	16	0.00010 ± 0.00003	

NSCLC: non-small cell lung cancer; TNM: tumor nodemetastases

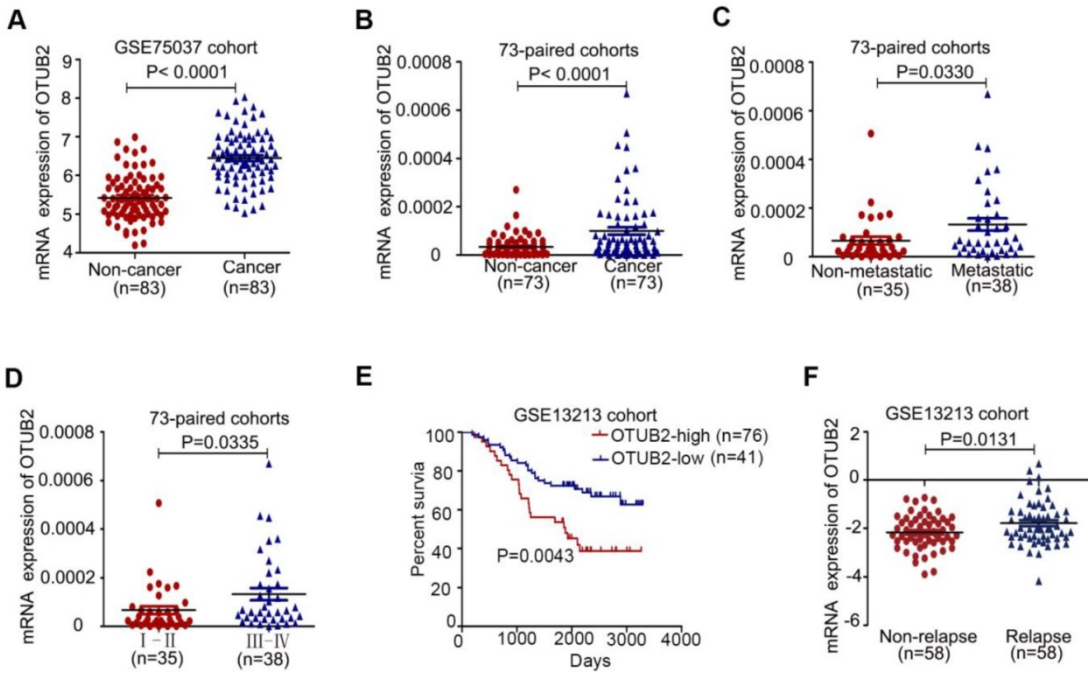

Figure 1. OTUB2 is upregulated in NSCLC and is associated with patient prognosis. (**A**) The levels of OTUB2 in 83 paired NSCLC tissues. (**B**) Real-time PCR analysis to quantify the levels of OTUB2 in 73 paired NSCLC tissues. (**C**) Real-time PCR analysis to quantify the levels of OTUB2 in NSCLC tissues with or without metastasis (lymph node metastasis and/or distal metastasis). (**D**) Real-time PCR analysis to quantify the levels of OTUB2 in patients with clinical early-stage (I-II) and advanced-stage (III-IV) NSCLC. (**E**) Correlation between OTUB2 levels and overall survival and (**F**) levels of OTUB2 in non-relapsed and relapsed lung cancer tissues. Statistical analysis was performed using Student's t-test in C, D and F; paired t-test in B; and Kaplan-Meier analyses in E. Error bars represent the SEM.

OTUB2 exerts tumor-stimulative functions of NSCLC cells

The mRNA and protein levels of OTUB2 were detected in NSCLC cell lines (**Figure 2A-B**). To investigate the functional roles of OTUB2 in NSCLC progression, we knocked down endogenous OTUB2 via two independent siRNAs in A549 and H1299 cells and established stable cell lines (HA-OTUB2) via lentiviral infection in XL-2 and H292 cells (**Figure 2C** and **Figure S2A**). Knockdown of OTUB2 significantly inhibited the proliferation and colony formation abilities of NSCLC cells compared with control cells (**Figure 2D, F**), whereas overexpression of OTUB2 substantially promoted the proliferation and colony formation abilities of NSCLC cells compared with control cells (**Figure 2E, G**). Moreover, knockdown of OTUB2 significantly suppressed the invasion and migration abilities of A549 and H1299 cells (**Figure 2H**). In contrast, stable overexpression of OTUB2 significantly increased the invasion and migratory abilities of XL-2 and H292 cells (**Figure 2I**). Similarly, knockdown of OTUB2 suppressed migration rates compared with the controls in A549 and H1299 cells (**Figure S2B**), and stable overexpression of OTUB2 enhanced the migration rates of XL-2 and H292 cells (**Figure S2C**). Taken together, these results demonstrate that OTUB2 acts as an important tumor promoter in NSCLC cells.

OTUB2 enhances the Warburg effect via the AKT/mTOR pathway

Cancer cells exhibit aberrant metabolism characterized by high glycolysis, even in the presence of abundant oxygen. This phenomenon, known as the Warburg effect or aerobic glycolysis, facilitates tumor growth with elevated glucose uptake and lactate production [31, 32]. To gain insight into the underlying mechanism of OTUB2 in NSCLC cells, we measured extracellular acidification rates (ECAR), which is indicative of glycolysis, in NSCLC cell lines. Knockdown of OTUB2 reduced the glycolytic capability of A549 and H1299 cells (**Figure 3A-B**). Consistent with this result, knockdown of OTUB2 led to a marked decrease in glucose uptake and extracellular lactate production in A549 and H299 cells (**Figure 3E**). Conversely, OTUB2 overexpression substantially enhanced glycolytic capability, glucose uptake and extracellular lactate production in XL-2 and H292 cells (**Figure 3C-D,** F). Meanwhile, we measured oxygen consumption rates (OCR), which is indicative of mitochondrial oxidative phosphorylation. OTUB2 overexpression had no impact on mitochondrial oxidative phosphorylation (**Figure S3A-B**). Western blot analysis confirmed the expression of 11 glycolysis-related enzymes (GLUT1, HK2, GPI, PFKL, ALDOA, GAPDH, PGK1, PGAM1, ENO1, PKM2, and LDHA) (**Figure 3G**). OTUB2 did

not markedly alter the expression of most glycolytic enzymes except for HK2, PFKL, PGK1, and PGAM1. Decreased expression of OTUB2 downregulated the expression of PGK1 and PGAM1 in both A549 and H1299 cells and downregulated the expression of HK2 and PFKL in A549 cells only. Overexpression of OTUB2 upregulated the expression of PFKL and PGK1 in H292 cells and upregulated the expression of HK2, PFKL, PGK1, and PGAM1 in XL-2 cells (**Figure 3H** and **Figure S3C-E**).

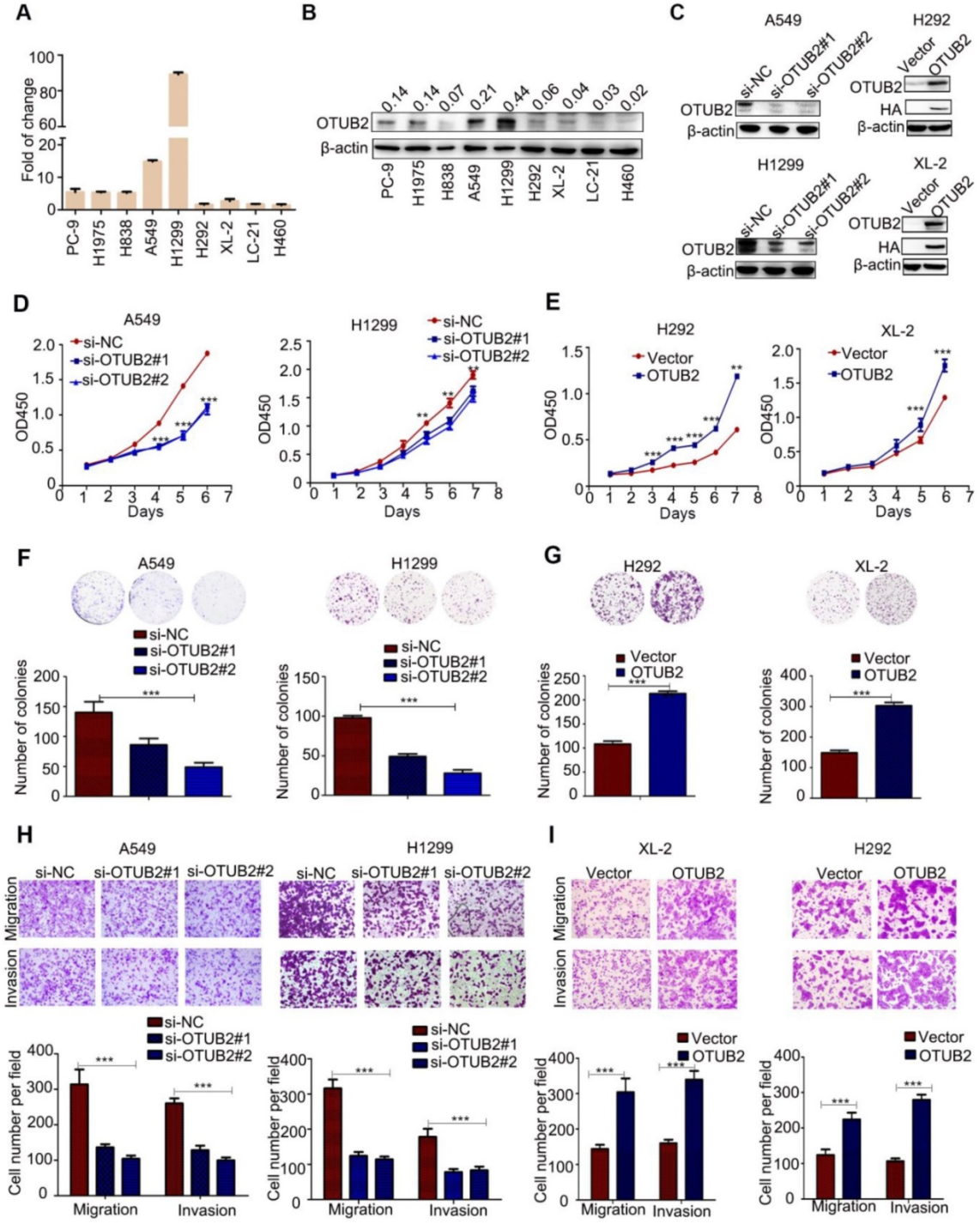

Figure 2. OTUB2 increases NSCLC cell proliferation, colony formation, migration and invasion in vitro. (**A**) OTUB2 was measured in different NSCLC cells by real-time PCR. (**B**) OTUB2 was measured in different NSCLC cells by Western blot. (**C**) OTUB2 was measured by Western blot in H292 and XL-2 cells stably expressing HA-OTUB2 and in A549 and H1299 cells transfected with two independent OTUB2 siRNAs. (D) CCK-8 assays in A549 and H1299 cells transfected with two independent OTUB2 siRNAs. (E) CCK-8 assays in stably expressing HA-OTUB2 XL-2 and H292 cells. (F) Colony formation assays in A549 and H1299 cells transfected with two independent OTUB2 siRNAs (magnification, ×40). (G) Colony formation assays in stably expressing HA-OTUB2 XL-2 and H292 cells (magnification, ×40). (H) Transwell migration and invasion assays in A549 and H1299 cells transfected with two independent OTUB2 siRNAs (magnification, ×200). (I) Transwell migration and invasion assays in stably expressing HA-OTUB2 XL-2 and H292 cells (magnification, ×200). Statistical analysis was performed using Student's t-test. Error bars represent the SEM. *P<0.05; ** P<0.01; *** P<0.001.

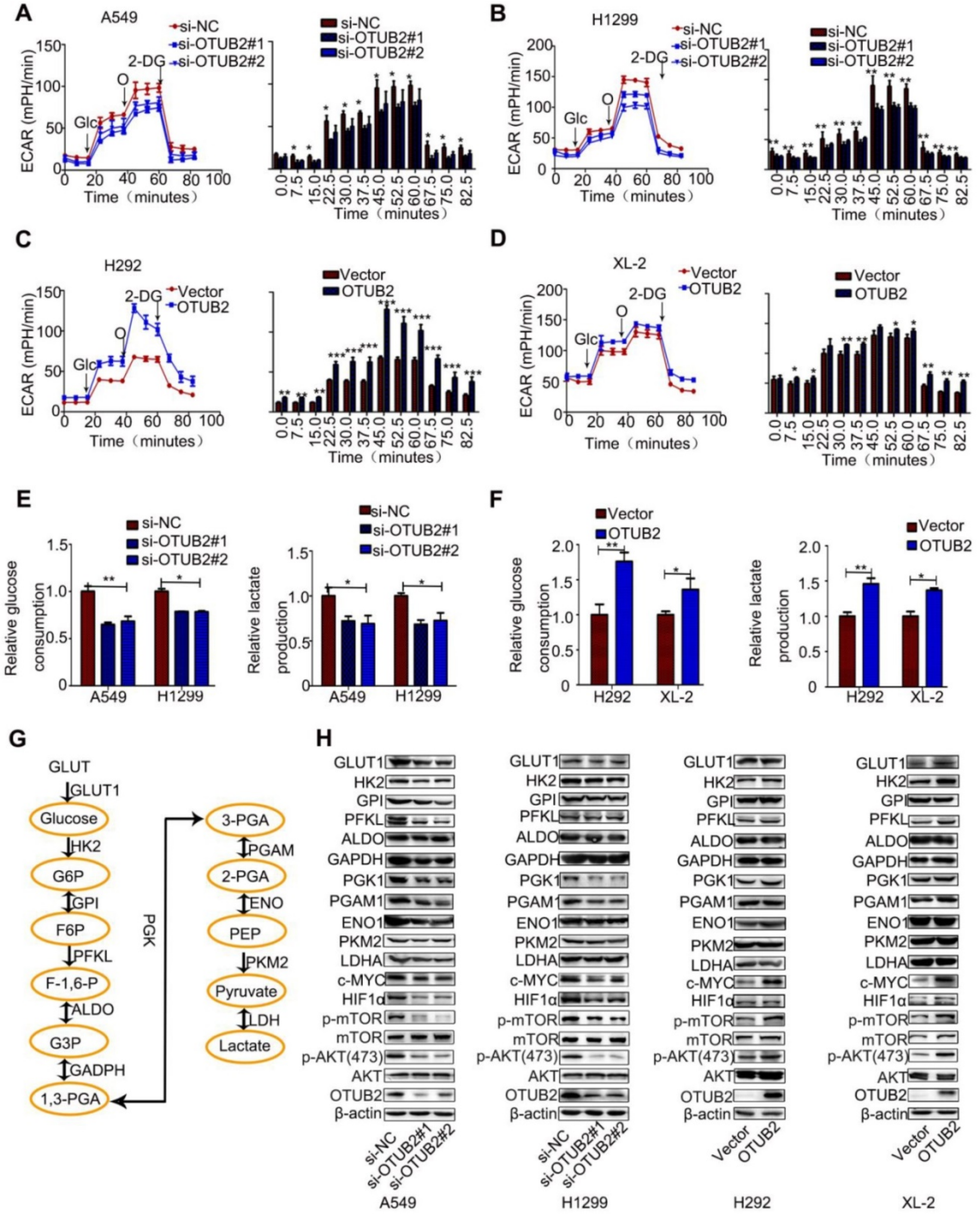

Figure 3. OTUB2 facilitates NSCLC cell survival by modulating the Warburg effect. (**A**-**B**) Extracellular acid ratio (ECAR) in A549 and H1299 cells transfected with OTUB2 siRNAs (left panel). Glc: glucose; O: oligomycin; 2-DG:2-deoxyglucose. A histogram of ECAR result is shown (right panel). (**C**-**D**) Extracellular acid ratio (ECAR) in stably expressing HA-OTUB2 XL-2 and H292 cells (left panel). A histogram of ECAR result is shown (right panel). (**E**) Glucose consumption and lactate production in A549 and H1299 cells transfected with OTUB2 siRNAs. (**F**) Glucose consumption and lactate production in stably expressing HA-OTUB2 XL-2 and H292 cells. (**G**) Schematic diagram of the aerobic glycolysis pathway. (**H**) Protein levels of aerobic glycolysis enzymes, c-Myc, HIF1a, and phosphorylated and total mTOR and AKT following knockdown or overexpression of OTUB2. Statistical analysis was performed using Student's t-test. Error bars represent the SEM. *P<0.05; ** P<0.01; *** P<0.001.

c-Myc and HIF1a are two crucial factors involved in the regulation of the Warburg effect by targeting glycolytic enzymes [33, 34]. OTUB2 may stimulate the Warburg effect by regulating HIF1a and c-Myc in NSCLC cells. To address this hypothesis, we first determined whether OTUB2 regulated HIF1a and c-Myc expression. OTUB2 knockdown remarkably decreased both HIF1a and c-Myc protein levels in NSCLC cells. Conversely, overexpression of OTUB2 substantially increased both HIF1a and c-Myc protein

levels in NSCLC cells (**Figure 3H** and **Figure S3C-E**). Collectively, these data indicate that OTUB2 promotes the Warburg effect by modulating HIF1a and c-Myc. We also examined the activity of mTOR signaling, which is influenced by intracellular fuel and energy status [35]**.** The phosphorylation levels of mTOR and AKT were increased, indicating that the mTOR pathway may be activated by OTUB2 (**Figure 3H** and **Figure S3C-E**). These data indicate that OTUB2 is a key regulator of the Warburg effect in NSCLC cells.

OTUB2 stabilizes U2AF2 in NSCLC cells

Cancer metabolism is regulated by a complicated network constituted of different means under various contexts instead of a straightforward single pathway operation [36]. Indeed, while we demonstrated that OTUB2 regulated PGK1, PGAM1, c-Myc, and HIF1a, we did not observe a direct interplay between these proteins. Next, to elucidate the underlying mechanism by which OTUB2 promotes NSCLC progression, a co-immunoprecipitation assay using antibodies against HA was performed in both 293T cells transfected with HA-tagged OTUB2 and control cells. The results revealed two specific bands at approximately 60 kD and 45 kD (**Figure 4A** and **Table S3**). After protein identification by mass spectrometry, five proteins (RPL3, TRIM21, PTBP1, RCC2, and U2AF2) were chosen for further verification based on their unique peptides (>4) and location in the nucleus (https://www.uniprot.org/uniprot). To assess the interactions between these proteins, we performed immunoprecipitation and Western blot analyses, and the results revealed that only U2 small nuclear RNA auxiliary factor 2 (U2AF2, also called U2AF65) co-immunoprecipitated with OTUB2 protein in HA-OTUB2-293T cells (**Figure 4B** and **Figure S4A**). The interaction between OTUB2 and U2AF2 was verified by co-immunoprecipitation assays in HA-OTUB2-H292 cells (**Figure 4B**). In addition, immunoprecipitation assays using an antibody against endogenous OTUB2 revealed endogenous interactions between OTUB2 and U2AF2 (**Figure 4C**). Furthermore, the interaction between endogenous OTUB2 and U2AF2 was demonstrated by co-immunoprecipitation using an antibody against endogenous U2AF2 in A549 and H1299 cells (**Figure 4D**). These results indicate that OTUB2 specifically interacts with U2AF2 in NSCLC cells.

It is unclear whether OTUB2, as a deubiquitinating enzyme, regulates U2AF2 ubiquitination. We first examined the mRNA and protein levels of U2AF2 following OTUB2 knockdown or overexpression in MG132-treated NSCLC cell lines wherein global proteasomal activity was inhibited. Knockdown of OTUB2 significantly inhibited the U2AF2 protein levels in A549 and H1299 cells (**Figure 4E**) but had no impact on U2AF2 mRNA levels (**Figure S4B**). Overexpression of OTUB2 substantially increased the U2AF2 protein levels in XL-2 and H292 cells (**Figure 4F**). To verify whether OTUB2 stabilizes U2AF2 protein, we examined the effect of both OTUB2 depletion and overexpression on the stability of endogenous U2AF2 protein in the presence of the protein synthesis inhibitor, cycloheximide (CHX). The half-life of U2AF2 protein was markedly reduced in OTUB2-knockdown cells compared to control cells in A549 and H1299 cells. Consistently, OTUB2 overexpression in XL-2 and H292 cells increased the half-life of U2AF2 protein in the presence of CHX (**Figure 4G**). These data collectively suggest that OTUB2 interacts with and stabilizes U2AF2 in NSCLC cells. Next, we determined which types of polyubiquitin modifications on U2AF2 protein are affected by OTUB2-mediated deubiquitination. Immunoprecipitation and Western blot analyses were performed with the U2AF2 antibody. OTUB2 knockdown significantly enhanced the levels of U2AF2 ubiquitination and K48-linked polyubiquitin chains in H1299 cells, whereas OTUB2 overexpression significantly reduced the levels of U2AF2 ubiquitination and K48-linked polyubiquitin chains in XL-2 cells (**Figure 4H**). The approach did not have an appreciable impact on the levels of K63-linked polyubiquitin-modified chains (**Figure S4C**). To identify whether OTUB2 deubiquitinated U2AF2 directly, we established HA-OTUB2^{C51S}, a mutant that is defective in DUB activity [23]. We incubated ubiquitinated U2AF2, purified from 293T cells,with either OTUB2 or OTUB2^{C51S},purified separately from 293T cells *In vitro*. Ubiquitinated U2AF2 was decreased by OTUB2 but not OTUB2^{C51S} (**Figure 4I**). This finding led us to hypothesize that OTUB2 directly interacts with and deubiquitinates U2AF2.

U2AF2, a direct target of OTUB2, is essential for OTUB2-mediated NSCLC progression

To investigate the functional roles of U2AF2 in OTUB2-mediated NSCLC progression, we knocked down endogenous U2AF2 via two independent siRNAs in A549 and H1299 cells (**Figure 5A** and **Figure S5A**). Similar effects were observed between OTUB2 and U2AF2 in NSCLC cells. Knockdown of U2AF2 significantly inhibited the proliferation, migration, and invasion abilities of A549 and H299 cells (**Figure 5B-D**). In addition, silencing U2AF2 significantly reduced glycolytic capability, glucose uptake, and extracellular lactate production in A549 and H299 cells (**Figure 5E-G**). Moreover, knockdown of U2AF2 showed markedly reduced PGK1, PGAM1,

HIF1a, c-Myc, p-AKT, and p-mTOR protein levels compared with control cells, but knockdown of U2AF2 showed markedly reduced PFKL levels in A549 cells only (**Figure 5H** and **Figure S5B-C**). Importantly, knockdown of U2AF2 rescued the promoting effect of OTUB2 on H292 cell migration and invasion (**Figure S5D-E**). In addition, the TIMER database (http://cistrome.org/timer) also showed that U2AF2 was increased in various human cancers (**Figure S6A**). Taken together, these results demonstrate that OTUB2 regulates proliferation, migration, invasion, and glycolysis in NSCLC cells via U2AF2.

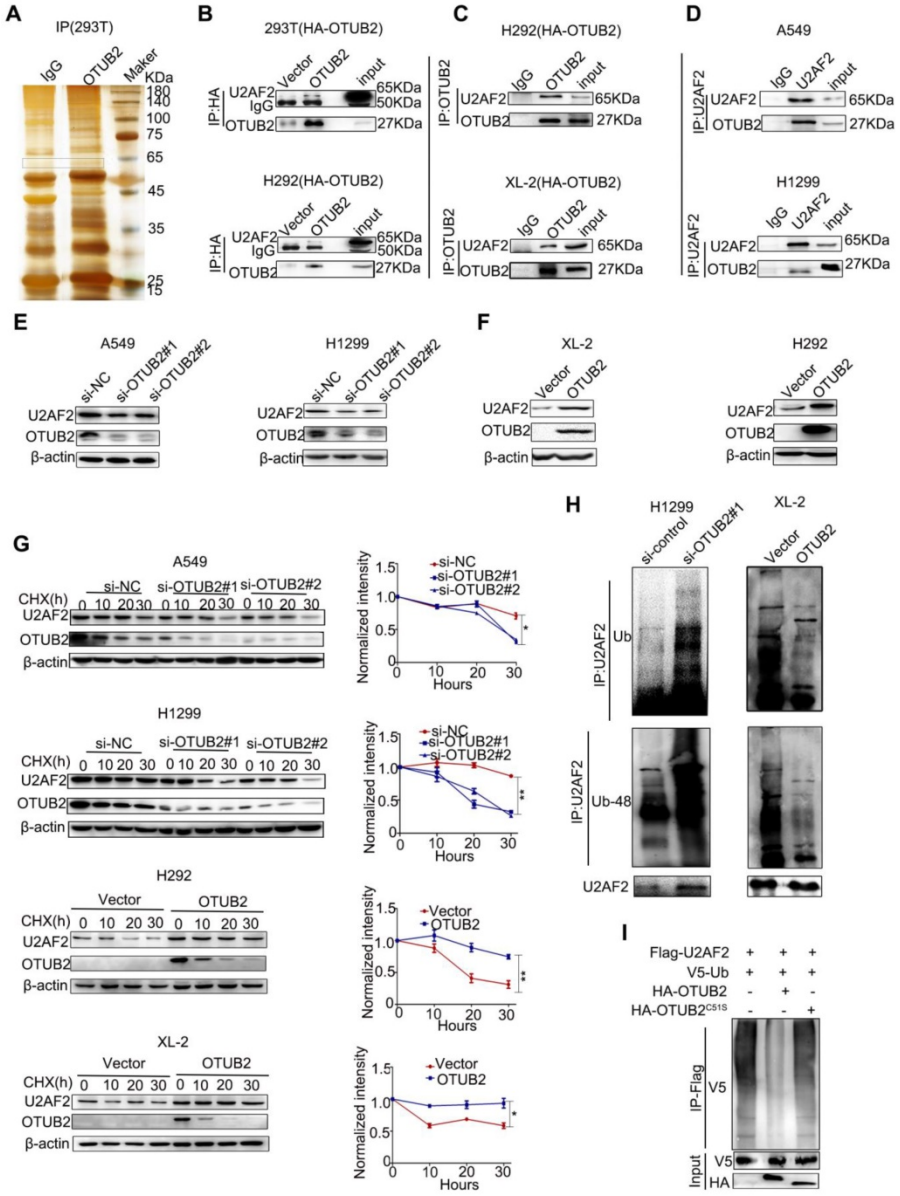

Figure 4. OTUB2 physically interacts with and stabilizes U2AF2 in NSCLC cells. (**A**) The HA-OTUB2 vector was transfected into HEK293T cells, and anti-HA was used to immunoprecipitate OTUB2-binding proteins. After silver staining, the 45 kD and 60 kD OTUB2-specific bands (arrows) were excised and analyzed by mass spectrometry. (**B**) Immunoprecipitation was carried out using an anti-HA antibody, and specific associations between U2AF2 and OTUB2 were analyzed by Western blotting in HEK293T and H292 cells transfected with plasmids encoding HA-tagged OTUB2. (**C**) Interaction between transfected HA-OTUB2 and endogenous U2AF2. Lysates from XL-2 and H292 cells expressing HA-OTUB2 were subjected to immunoprecipitation/Western blot analysis using anti-OTUB2. (**D**) Interaction between endogenous OTUB2 and U2AF2. Lysates from A549 and H1299 cells were subjected to immunoprecipitation/Western blot analysis using anti-OTUB2. (**E**) Western blotting was used to detect U2AF2 in A549 and H1299 cells transfected with OTUB2 siRNAs. (**F**), Western blotting was used to detect U2AF2 in stably expressing HA-OTUB2 XL-2 and H292 cells. (**G**) A549 and H1299 cells transfected with OTUB2 siRNAs and control siRNA. XL-2 and H292 cells with or without stable expression of HA-OTUB2 were treated with CHX (100 μg/ml) for the indicated time points. The cell lysates were examined by immunoblotting (left panel). A plot of the normalized amount of U2AF2 protein is shown (right panel). The quantification of U2AF2 levels relative to β-actin is shown. (**H**) H1299 cells with OTUB2 knockdown and XL-2 cells overexpressing HA-OTUB2. Different forms of ubiquitin were treated with MG132 (10 μM) for 20 h. Cell lysates were immunoprecipitated using control IgG or a U2AF2 antibody and then immunoblotted for ubiquitin and K48-ubiquitin. (**I**) In vitro ubiquitination assay. Purified V5-ubiquitin, Flag-U2AF2 was incubated with HA-OTUB2 or HA-OTUB2^{C51S} for 1 h in the reaction buffer. After the reaction, Flag-U2AF2 proteins were further purified with anti-Flag antibody and immunoblotted with antibodies against V5 and Flag. Statistical analysis was performed by one-way ANOVA. Error bars represent the SEM. *P<0.05; ** P<0.01; ***P<0.001.

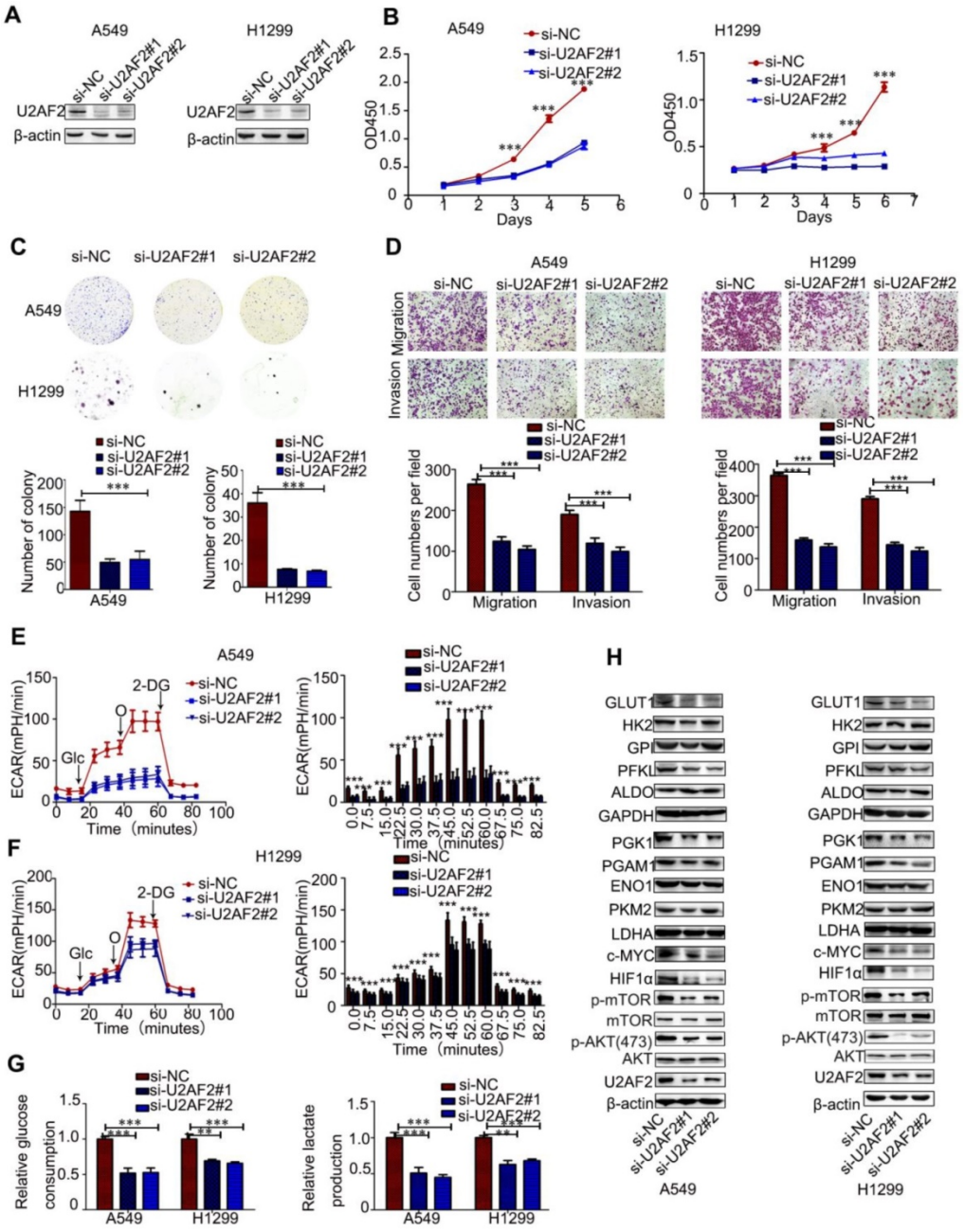

Figure 5. U2AF2 is the functional downstream target of OTUB2 in NSCLC. (**A**) Immunoblotting for U2AF2 protein levels in A549 and H1299 cells transfected with two independent U2AF2 siRNAs. (**B**) CCK-8 assays in A549 and H1299 cells transfected with U2AF2 siRNAs. (**C**) Colony formation assays in A549 and H1299 cells transfected with U2AF2 siRNAs. (**D**) Transwell migration and invasion assays in A549 and H1299 cells transfected with U2AF2 siRNAs (magnification, ×200). (**E-F**) ECAR in A549 and H1299 cells transfected with U2AF2 siRNAs (left panel). A histogram of ECAR result is shown (right panel). (**G**) Glucose consumption and lactate production in A549 and H1299 cells transfected with U2AF2 siRNAs. (**H**) Protein levels of aerobic glycolysis enzymes, c-Myc, HIF1a, and phosphorylated and total mTOR and AKT in A549 and H1299 cells transfected with U2AF2 siRNAs. β-actin served as the internal control. Statistical analysis was performed using Student's t-test. Error bars represent the SEM. *P<0.05; ** P<0.01; ***P<0.001.

U2AF2 is upregulated in NSCLCs and correlates with OTUB2 levels

To further delineate whether OTUB2-mediated regulation of U2AF2 expression is clinically relevant to human NSCLC development, we compared U2AF2 expression in 83 paired NSCLC samples and detected U2AF2 was upregulated in lung cancer tissues (GEO Submission: GSE75037) (**Figure 6A**). Real-time PCR analysis was employed to confirm elevated U2AF2 expression in 73 NSCLCs compared with their adjacent non-tumor tissues (**Figure 6B** and **Table 2**). Clinical association studies have found that U2AF2 expression was significantly associated with lymph node and distal metastasis (P<0.001), advanced TNM stages (P=0.0014), and larger tumor size (P=0.0280) (**Figure 6C-E** and **Table 2**). Importantly, Kaplan-Meier's survival analysis showed that U2AF2

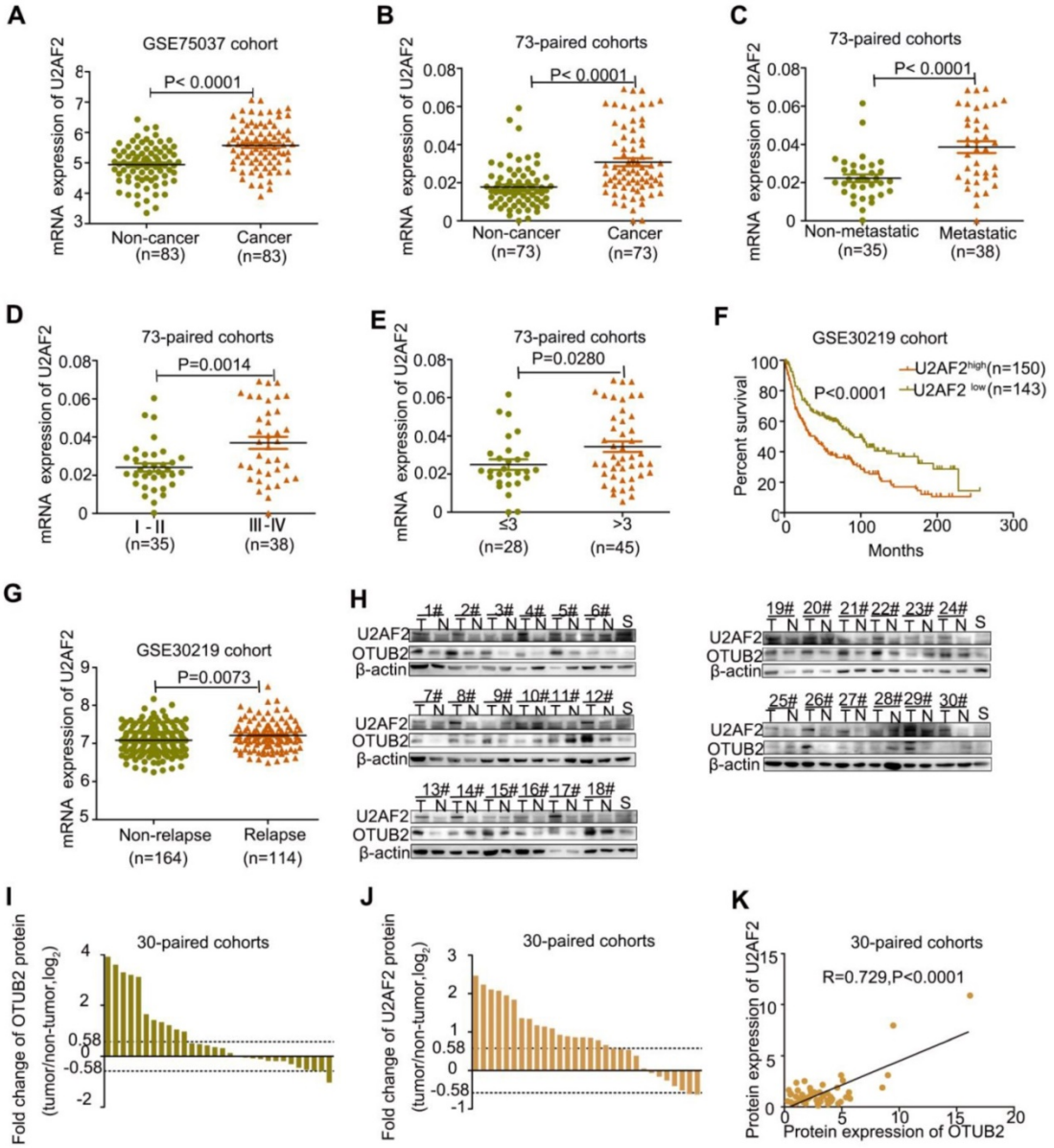

Figure 6. U2AF2 is upregulated in NSCLCs and correlates with OTUB2 levels. (**A**) The levels of U2AF2 in 83 paired NSCLC tissues. (**B**) Real-time PCR analysis to quantify the levels of U2AF2 in 73 paired NSCLC tissues. (**C**) Real-time PCR analysis to quantify the levels of U2AF2 in NSCLC tissues with or without metastasis (lymph node metastasis and/or distal metastasis). (**D**) Real-time PCR analysis to quantify the levels of U2AF2 in patients with clinical early-stage (I-II) and advanced-stage (III -IV) NSCLC. (**E**) Real-time PCR analysis to quantify the levels of U2AF2 in patients with tumor volume (≤3) and (>3). (**F**) Correlation between U2AF2 levels and overall survival in 284 lung cancer patients. (**G**) Levels of U2AF2 in non-relapsed and relapsed lung cancer tissues in 284 lung cancer patients. (**H**) Photos of representative blots for OTUB2 and U2AF2 expression in 30 pairs of lung cancer and noncancerous tissues. (**I**) Fold changes in OTUB2 expression in 30 paired NSCLC tissues. (**J**) Foldchanges in U2AF2 expression in 30 paired NSCLC tissues. (**K**) Correlation between OTUB2 and U2AF2 expression in NSCLC samples. β-actin was used as a loading control. Statistical analysis was performed using Student's t-test in C, D, E and G; paired t-test in B; Kaplan-Meier analyses in F; and Spearman's correlation test in K. Error bars represent the SEM. *P<0.05; ** P<0.01; ***P<0.001.

expression negatively correlated with overall survival (OS) in 293 NSCLC patients (GEO Submission: GSE30219), but not in 117 NSCLC patients (GEO Submission: GSE13213) (**Figure 6F** and **Figure S6B**). By comparing U2AF2 expression between NSCLC patients with and without relapse, we found that U2AF2 was increased in relapsed patients in both GSE30219 and GSE13213 (**Figure 6G** and **Figure S6C**). In addition, Western blot analyses showed elevated OTUB2 and U2AF2 protein expression in 30 NSCLCs compared with their adjacent non-tumor tissues (**Figure 6H-J**). Importantly, a positive correlation between OTUB2 and U2AF2 was found (P<0.001 by Spearman's correlation test; **Figure 6K**). An additional paired chi square test was performed to prove the positive correlation between OTUB2 and U2AF2 (**Table S4**). These results suggest that U2AF2 plays an important role in OTUB2-mediated NSCLC progression.

OTUB2 promotes xenograft tumor growth of NSCLC cell via stabilizing U2AF2 and enhancing the Warburg effect *In vivo*

To further investigate the effect of OTUB2 on tumor growth *In vivo*, XL-2 cells with stable OTUB2 overexpression (OTUB2 group) and control XL-2 cells (vector group) were transplanted into nude mice subcutaneously. The size and weight of the tumors formed by XL-2 cells with stable OTUB2 overexpression were significantly increased in comparison with the tumors formed by control XL-2 cells (**Figure 7A-C**). We further performed Western blot to detect the protein expression of 11 glycolysis-related enzymes, as well as U2AF2, HIF1a, c-Myc, mTOR, AKT, p-mTOR and p-AKT in xenograft tumor tissues. Compared with the tumors formed by control XL-2 cells, the tumors formed by XL-2 cells with stable OTUB2 overexpression showed markedly increased U2AF2, GLUT1, HK2, PGK1, PGAM1, HIF1a, c-Myc, p-AKT, and p-mTOR protein levels. These results are similar to the *In vitro* results (**Figure 7D-E**). However, overexpression of OTUB2 showed a decrease in GAPDH and GPI levels. This phenomenon, inconsistent with *In vitro* experiments, may be due to the differences between *In vitro* and *In vivo* experiments. Taken together, these results indicate that OTUB2 promotes xenograft tumor growth of NSCLC cells by stabilizing U2AF2 and enhancing the Warburg effect *In vivo*.

Table 2. Correlation between U2AF2 levels in NSCLC patients and their clinicopathologic characteristics

Clinicopathologic parameters	Number of cases	Median expression of U2AF2	
		Mean±SD	P-value
Age (year)			
≤60	31	0.0308 ± 0.0029	0.9603
>60	42	0.0306 ± 0.0030	
Gender			
Male	44	0.0301 ± 0.0027	0.7121
Female	29	0.0317 ± 0.0033	
Tumor size(cm)			
≤3	28	0.0249 ± 0.0027	0.0259*
>3	45	0.0343 ± 0.0028	
TNM stage			
Stage I + II	35	0.0240 ± 0.0021	0.0014**
Stage III+IV	38	0.0369 ± 0.0032	
Metastasis			
No	35	0.0222 ± 0.0020	< 0.0001***
Yes	38	0.0386 ± 0.0031	
Carcinoma			
NSCLC	73	0.0307 ± 0.0021	< 0.0001***
Adjacent Lung	73	0.0177 ± 0.0013	
Pathologic classification			
Adenocarcinoma	57	0.0030 ± 0.0041	0.8254
Squamous carcinoma	16	0.0031 ± 0.0024	

NSCLC: non-small cell lung cancer; TNM: tumor nodemetastases

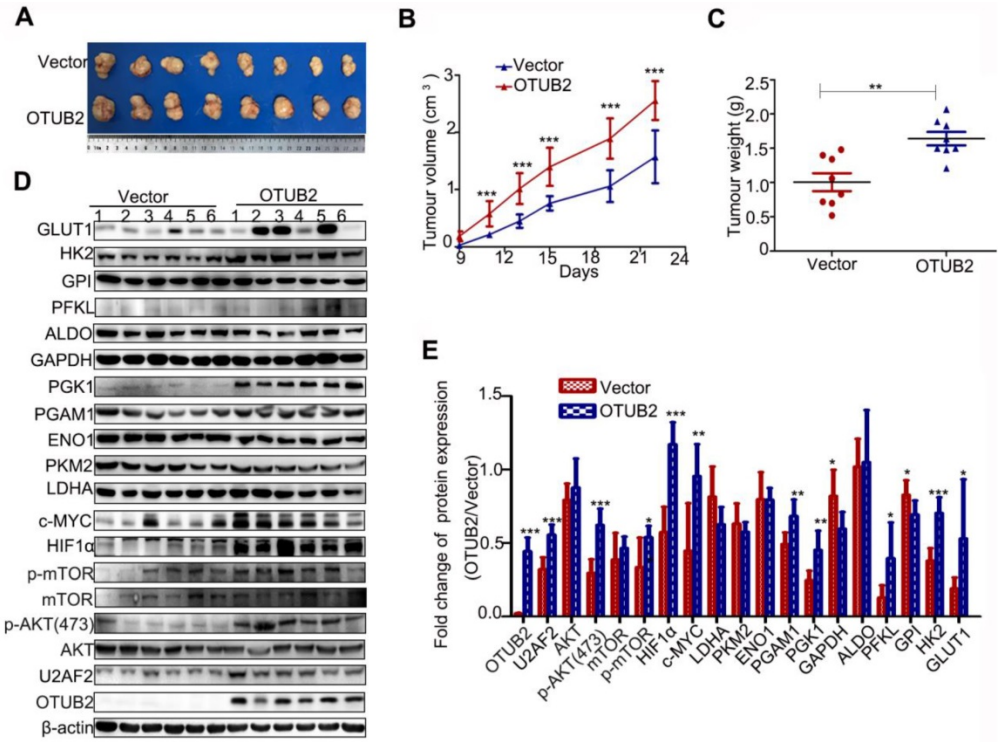

Figure 7. OTUB2 promotes xenograft tumor growth of NSCLC cell via stabilizing U2AF2 and enhancing the Warburg effect in vivo. (A). The xenograft tumors formed by OTUB2-overexpressed and control vector in XL-2 cells. **(B-C)** The size and weight of the xenograft tumors formed by OTUB2-overexpressed and control cells. **(D)** Protein levels of aerobic glycolysis enzymes, U2AF2, c-Myc, HIF1a, and phosphorylated and total mTOR and AKT in tumors formed by OTUB2-overexpressed and control cells. β-actin served as the internal control. **(E)** A histogram of Western blot result is shown. Statistical analysis was performed using Student's t-test. Error bars represent the SEM. *P<0.05; ** P<0.01; ***P<0.001.

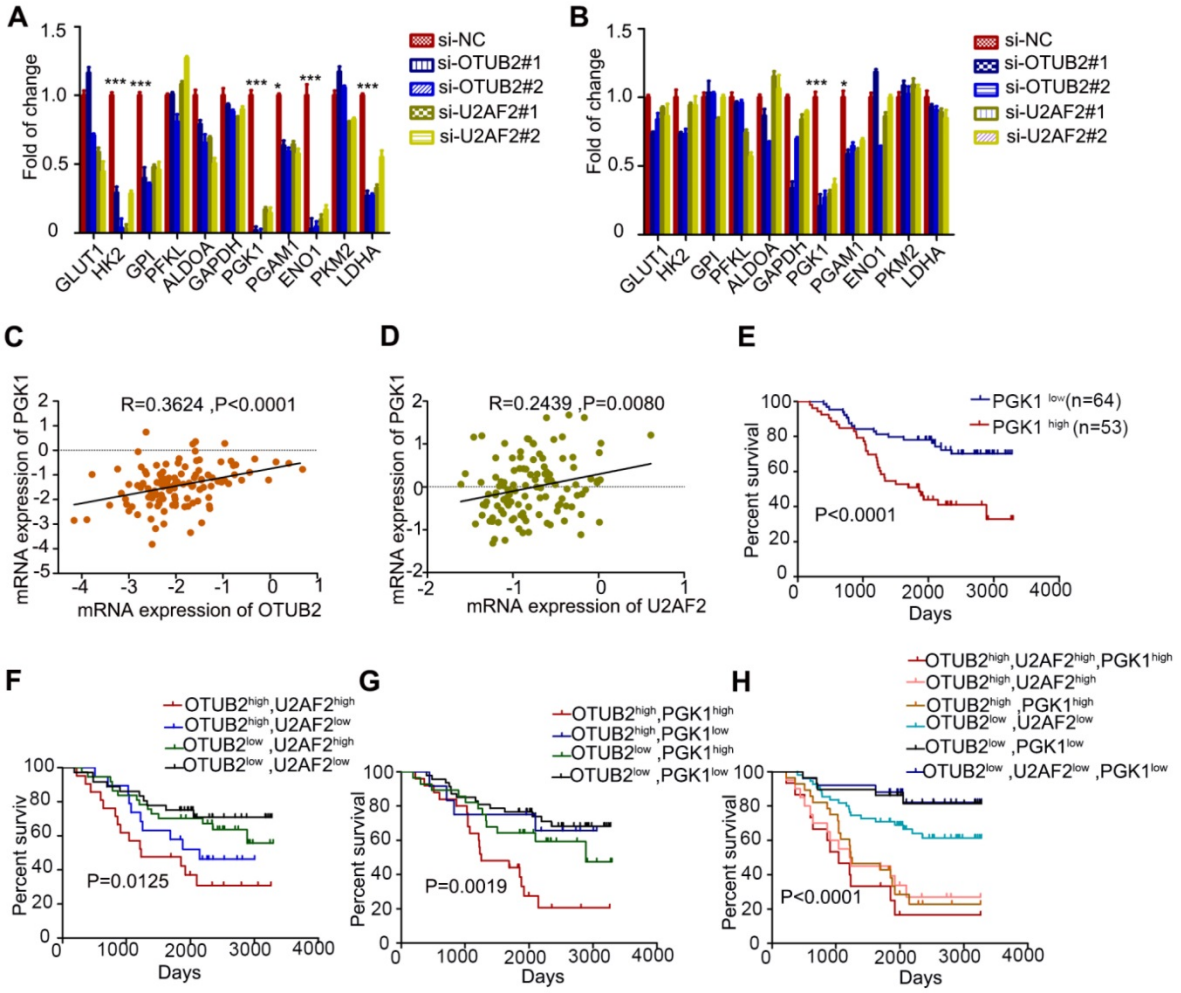

Figure 8. A combination of OTUB2, U2AF2 and PGK1 serves as a powerful prognostic factor for NSCLC patients. (**A**-**B**) Real-time PCR analyses of aerobic glycolysis enzymes expression in A549 and H1299 cells transfected with two independent OTUB2 and U2AF2 siRNAs. (**C**) Correlation between OTUB2 and PGK1 mRNA expression in 117 lung cancer patients. (**D**) Kaplan-Meier's survival analysis of the correlation between U2AF2 and PGK1 mRNA expression in 117 lung cancer patients (**E**) Kaplan-Meier's survival analysis of the correlation between PGK1 levels and overall survival in 117 lung cancer patients. (**F**) Kaplan-Meier's survival analysis of the correlation between the combination of OTUB2 and U2AF2 expression levels and overall survival in 117 lung cancer patients. (**G**) Kaplan-Meier's survival analysis of the correlation between the combination of OTUB2 and PGK1 expression levels and overall survival in 117 lung cancer patients. (**H**) Kaplan-Meier's survival analysis of the correlation between the combination of OTUB2, U2AF2 and PGK1 expression levels and overall survival in 117 lung cancer patients. Statistical analysis was performed using Student's t-test in A and B; Kaplan-Meier analyses in E-H; and Spearman's correlation test in C and D. Error bars represent the SEM. *P<0.05; ** P<0.01; ***P<0.001.

High expression of OTUB2, U2AF2 and PGK1 is significantly associated with worse prognosis in NSCLC patients

Compared to control cells, the knockdown of OTUB2 and U2AF2 showed significantly reduced mRNA expression of PGK1 and PGAM1 in A549 and H1299 cells, especially PGK1 by real-time PCR (**Figure 8A-B**). Further, we determined whether mRNA expression of PGK1 levels is associated with OTUB2 and U2AF2 levels in 117 NSCLC tissues. Increased OTUB2 and U2AF2 expression was positively correlated with PGK1 expression in NSCLC tissues (**Figure 8C-D**). Importantly, a univariate analysis showed that PGK1 expression negatively correlated with OS in 117 NSCLC patients (P < 0.001; **Figure 8E**). We also analyzed the prognostic value of combining OTUB2 and U2AF2, OTUB2 and PGK1, as well as OTUB2, U2AF2 and PGK1 levels in 117 NSCLC patients. As expected, OTUB2-U2AF2-high and OTUB2-PGK1-high patients had the worst OS, whereas OTUB2-U2AF2-low and OTUB2-PGK1-low patients had a better OS (P=0.0125; **Figure 8F** and P=0.0019; **Figure 8G**, respectively). Additionally, OTUB2-U2AF2-PGK1-high patients showed the worst OS, whereas OTUB2-U2AF2-PGK1-low patients had the best OS (P < 0.001; **Figure 8H**). OTUB2, U2AF2, and PGK1 that exhibited significant differences in a univariate analysis were included in a multivariate analysis. The Cox proportional hazards model showed a trend that OTUB2 (χ^2 =2.911, Risk Ratio = 1.306), U2AF2 (χ^2 = 1.601, Risk Ratio = 1.319) and PGK1 (χ^2 = 1.668, Risk Ratio = 1.551) were independent prognostic variables in NSCLC patients.

Because the sample size is too small, it is not statistically significant.

Discussion

Increasing evidence has confirmed that deubiquitinating enzymes play an important role in lung cancer progression. Our initial study first uncovered that OTUB2 is an oncogenic deubiquitinating enzyme in NSCLC cells. Moreover, we provided mechanistic insights into OTUB2 as an oncogenic AKT/mTOR pathway activator and a critical regulator of the Warburg effect via its interaction with U2AF2, thereby preventing its ubiquitination.

In the present study, we focused on OTUB2, which was significantly upregulated in NSCLC tissue samples compared with the corresponding non-cancerous tissues. Furthermore, high levels of OTUB2 in NSCLC tissues were associated with tumor metastasis and advanced TNM stages. We also confirmed that OTUB2 enhanced the proliferation, migration, and invasion abilities of NSCLC cells *In vitro*. These findings indicate that OTUB2 acts as a tumor promoter in carcinogenesis.

Cancer cells frequently display increased aerobic glycolysis, or the Warburg effect, which contributes to the aggressive traits of tumor cells by providing energy, including enhanced growth ability, increased metastatic capacity, and chemoresistance [32]. As expected, we verified that OTUB2 overexpression increased ECAR, glucose uptake, and lactate production, while knockdown of OTUB2 impaired the aerobic glycolytic phenotype in different NSCLC cell lines. There are 11 glycolysis-related genes in the glycolytic pathway [37]. We further found that OTUB2 regulates the expression of many glycolytic enzymes, such as PGK1 and PGAM1. PGK1, the first ATP-generating enzyme of the glycolytic pathway, catalyzes the transfer of high-energy phosphate from position 1 of 1,3- diphosphoglycerate (1,3-BPG) to ADP, which leads to the generation of 3-phosphoglycerate (3-PG) and ATP [38]. Moreover, PGAM1 catalyzes the conversion of 3-phosphoglycerate (3-PG) to 2-phosphoglycerate (2-PG) during glycolysis. PGK1 and PGAM1 are dysregulated in many cancers and modulate cancer cell proliferation, apoptosis and/or metastasis in NSCLC cells [39-46]. To our surprise, we also observed changes in HK2 and PFKL in A549, H292 and XL-2 cells, but not in H1299 cells. No change in PGAM1 was observed in H292 cells. Due to the complexity and heterogeneity of tumor cells, we speculate that the regulation of glycolysis-related enzymes by OTUB2 may not be identical in all NSCLC cell lines. Moreover, it was very intriguing for us to show that OTUB2 promoted the protein expression of HIF1a and c-Myc and induced activation of the AKT/mTOR pathway. c-Myc and HIF1a are two crucial factors involved in the regulation of the Warburg effect by targeting glycolytic enzymes [31, 47-49]. The AKT/mTOR signaling pathway serves as a central regulator of cell metabolism, growth, proliferation, and survival [50]. Taken together, the present study demonstrated that OTUB2 facilitates the Warburg effect and partially explains the role of this oncogenic protein in NSCLC cells.

Mechanistically, we compared the proteins that bind to OTUB2, which led to the discovery of U2AF2 as a target of OTUB2 in NSCLC cells. OTUB2 was also observed to bind to and deubiquitinate TRAF3, TRAF6, and L3MBTL1 [21, 51, 52]. Our data provide ample evidence to demonstrate that OTUB2 binds to U2AF2, efficiently deubiquitinating it by removing the K-48 polyubiquitin chains and protecting it from proteasomal degradation. The protein level of U2AF2 was notably decreased and its ubiquitination was significantly increased when OTUB2 was knocked down. In contrast, when OTUB2 was overexpressed in NSCLC cells, U2AF2 was upregulated and its ubiquitination was significantly decreased. Of note, U2AF2 deubiquitination by OTUB2 is important for U2AF2 stabilization. However, the molecular details of its regulation remain to be defined. One approach, using point mutants of these proteins that specifically disrupt the U2AF2/OTUB2 interaction, may deepen our understanding of the OTUB2 regulation of U2AF2. Designing such mutants is currently difficult owing to the lack of structural insights into the interaction but warrants future studies.

Precursor messenger RNA (pre-mRNA) splicing is a key post-transcriptional process in which intronic sequences are excised and exonic sequences are ligated together to form mature messenger RNA (mRNA). In humans, more than 90% of genes undergo alternative splicing, underscoring the fundamental importance of this regulatory process in expanding protein diversity [53-55]. The misregulation of alternative splicing is closely associated with various human diseases, including cancers [56-58]. U2AF2, also called U2AF65, has been implicated as a key regulator required for binding U2 small nuclear ribonucleoproteins (snRNP) to pre-mRNA in alternative splicing [59-62]. U2AF2 is also elevated in lung cancer and the highly metastatic hepatocellular carcinoma cell line. Overexpression of U2AF2 correlated with adverse OS and relapse-free survival (RFS) as well as T cell-infiltrating human colon cancer [63-65]. Our current findings suggest that OTUB2 promotes NSCLC progression, which is largely dependent on U2AF2, at least in NSCLC cells.

Several lines of evidence support this notion. First, knockdown of U2AF2 significantly reduced the proliferation, migration, and invasion abilities of NSCLC cells. Second, knockdown of U2AF2 reduced glycolytic capability, glucose uptake, and extracellular lactate production. Third, knockdown of U2AF2 reduced the protein levels of HIF1a, c-Myc, p-AKT, p-mTOR, PGK1, and PGAM1. Knockdown of U2AF2, however, did not reduce the expression of HK2 and PFKL. Thus, we cannot exclude the possibility that other proteins regulated by OTUB2 may also regulate the expression of glycolysis-related enzymes. Fourth, U2AF2 expression was positively correlated with cancer progression and negatively correlated with survival in NSCLC tissues. Importantly, a positive correlation between the protein expression of OTUB2 and U2AF2 was found in NSCLC tissues. , In fact, it has been revealed that U2AF2 is essential for the OTUB2-mediated Warburg effect and NSCLC progression. The molecular mechanisms of U2AF2 in alternative splicing in NSCLC remain unclear, however. It would be interesting to investigate the mechanisms by which U2AF2 exerts its stimulative effects on NSCLC in future studies.

In this study, we offer the first evidence that the OTUB2/U2AF2 axis is upregulated in cancer, which correlates with poor prognosis in NSCLC patients. We also indicate a causal role for the OTUB2/U2AF2 axis in NSCLC progression (**Figure 9**). The current findings shed some light on the relationships between deubiquitination, RNA splicing machinery and glucose metabolism pathway to elucidate how NSCLC cells utilize glucose to promote their growth and migration. Further studies will likely lead to a new strategy for cancer therapy.

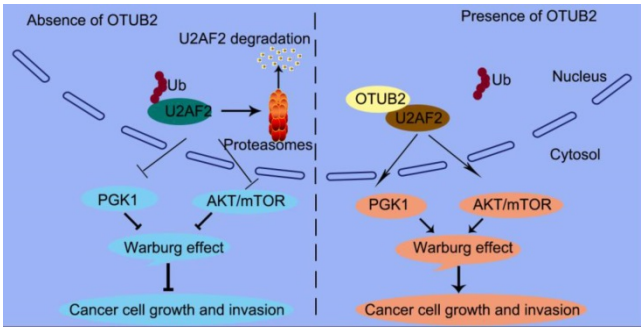

Figure 9. A proposed model underlying the OTUB2/U2AF2 axis as an activator of the Warburg effect and tumorigenesis in NSCLC cells. The working model shows that OTUB2 exerts its oncogenic activity by interacting with and stabilizing U2AF2, thereby upregulating glycolysis-related proteins and activating AKT/mTOR signaling in NSCLC cells.

Abbreviations

AD: adenocarcinoma; DUBs: deubiquitinating enzymes; ECAR: extracellular acidification rate; GEO: gene expression omnibus; JAMMs: Josephins and JAB1/MPN/MOV34 metalloenzymes; NSCLC: non-small cell lung cancer; OCR: oxygen consumption rate; OTUs: ovarian tumor-like proteases; PVDF: polyvinylidene fluoride; SCC: squamous cell carcinoma; SDS-PAGE: sodium dodecyl sulphate-polyacrylamide gel electrophoresis; snRNP: small nuclear ribonucleoproteins; TNM: tumor node metastases. UCHs: ubiquitin carboxyl-terminal hydrolases; UPS: ubiquitin-proteasome system; USPs: ubiquitin-specific proteases.

Supplementary Material

Supplementary figures and tables.
http://www.thno.org/v09p0179s1.pdf

Acknowledgements

This work was funded by the Shanghai Jiao Tong University School of Medicine Doctoral Innovation Foundation (BXJ201822), National Natural Science Foundation of China (81802894, 81702846), and Shanghai Health and Family Planning Commission Research fund (20174Y0183).

Competing Interests

The authors have declared that no competing interest exists.

References

1. Torre LA, Bray F, Siegel RL et al. Global cancer statistics, 2012. CA Cancer J Clin. 2015; 65: 87-108.
2. Jiang T , Li XF 2 , Wang JF et al. Mutational Landscape of cfDNA Identifies distinct molecular features associated with therapeutic response to first-line platinum-based doublet chemotherapy in patients with advanced NSCLC. Theranostics. 2017; 7: 4753-62.
3. Jemal A, Ward EM, Johnson CJ et al. Annual report to the nation on the status of cancer, 1975-2014, featuring survival. J Natl Cancer Inst. 2017; 109: PMID:28376154.
4. Chen W, Zheng R, Baade PD et al. Cancer statistics in China, 2015. CA Cancer J Clin. 2016; 66: 115-32.
5. Dela Cruz CS, Tanoue LT, Matthay RA. Lung cancer: epidemiology, etiology, and prevention. Clin Chest Med. 2011; 32: 605-44.
6. Leon S, Haguenauer-Tsapis R. Ubiquitin ligase adaptors: regulators of ubiquitylation and endocytosis of plasma membrane proteins. Exp Cell Res. 2009; 315: 1574-83.
7. Hicke L. Protein regulation by monoubiquitin. Nat Rev Mol Cell Biol. 2001; 2: 195-201.
8. Ventii KH, Wilkinson KD. Protein partners of deubiquitinating enzymes. Biochem J. 2008; 414: 161-75.
9. Fraile JM, Quesada V, Rodriguez D et al. Deubiquitinases in cancer: new functions and therapeutic options. Oncogene. 2012; 31: 2373-88.
10. Pijnappel WW, Timmers HT. Dubbing SAGA unveils new epigenetic crosstalk. Mol Cell. 2008; 29: 152-4.
11. Zhang Y. Transcriptional regulation by histone ubiquitination and deubiquitination. Genes Dev. 2003; 17: 2733-40.
12. Uckelmann M, Densham RM, Baas R et al. USP48 restrains resection by site-specific cleavage of the BRCA1 ubiquitin mark from H2A. Nat Commun. 2018; 9: 229.
13. Das DS, Das A, Ray A et al. Blockade of deubiquitylating enzyme USP1 inhibits DNA repair and triggers apoptosis in multiple myeloma cells. Clin Cancer Res. 2017; 23: 4280-9.
14. Li Y, Luo K, Yin Y et al. USP13 regulates the RAP80-BRCA1 complex dependent DNA damage response. Nat Commun. 2017; 8: 15752.
15. Kwasna D, Abdul Rehman SA, Natarajan J et al. Discovery and characterization of ZUFSP/ZUP1, a distinct deubiquitinase class important for genome stability. Mol Cell. 2018; 70(e6): 150-64.
16. Chen X, Yu C, Gao J et al. A novel USP9X substrate TTK contributes to tumorigenesis in non-small-cell lung cancer. Theranostics. 2018; 8:2348-60.

17. Sun SC. Deubiquitylation and regulation of the immune response. Nat Rev Immunol. 2008; 8: 501-11.
18. Yuan L, Lv Y, Li H et al. Deubiquitylase OTUD3 regulates PTEN stability and suppresses tumorigenesis. Nat Cell Biol. 2015;17:1169-81.
19. Wang B, Jie Z, Joo D et al. TRAF2 and OTUD7B govern a ubiquitin-depende-nt switch that regulates mTORC2 signalling. Nature. 2017; 545: 365-9.
20. Nanao MH, Tcherniuk SO, Chroboczek J et al. Crystal structure of human otubain 2. EMBO Rep. 2004; 5: 783-8.
21. Li S, Zheng H, Mao AP et al. Regulation of virus-triggered signaling by OTUB1- and OTUB2-mediated deubiquitination of TRAF3 and TRAF6. J Biol Chem. 2010; 285: 4291-7.
22. Beck A, Vinik Y, Shatz-Azoulay H et al. Otubain 2 is a novel promoter of beta cell survival as revealed by siRNA high-throughput screens of human pancreatic islets. Diabetologia. 2013; 56: 1317-26.
23. Kato K, Nakajima K, Ui A et al. Fine-tuning of DNA damage-dependent ubiquitination by OTUB2 supports the DNA repair pathway choice. Mol Cell. 2014; 53: 617-30.
24. Johmura Y, Yamashita E, Shimada M et al. Defective DNA repair increases susceptibility to senescence through extension of Chk1-mediated G2 checkpoint activation. Sci Rep. 2016; 6: 31194.
25. Cui YQ, Geng Q, Yu T et al. Establishment of a highly metastatic model with a newly isolated lung adenocarcinoma cell line. Int J Oncol. 2015; 47: 927-40.
26. Yu T, Li J, Yan M et al. MicroRNA-193a-3p and -5p suppress the metastasis of human non-small-cell lung cancer by downregulating the ERBB4/PIK3R3/mTOR/S6K2 signaling pathway. Oncogene. 2015; 34: 413-23.
27. Zhou Y, Wu J, Fu X et al. OTUB1 promotes metastasis and serves as a marker of poor prognosis in colorectal cancer. Mol Cancer. 2014; 13: 258.
28. Iglesias-Gato D, Chuan YC, Jiang N et al. OTUB1 de-ubiquitinating enzyme promotes prostate cancer cell invasion in vitro and tumorigenesis in vivo. Mol Cancer. 2015; 14: 8.
29. Weng W, Zhang Q, Xu M et al. OTUB1 promotes tumor invasion and predicts a poor prognosis in gastric adenocarcinoma. Am J Transl Res. 2016; 8: 2234-44.
30. Baietti MF, Simicek M, Abbasi Asbagh L et al. OTUB1 triggers lung cancer development by inhibiting RAS monoubiquitination. EMBO Mol Med. 2016; 8: 288-303.
31. Liberti MV, Locasale JW. The Warburg Effect: How Does it Benefit Cancer Cells? Trends Biochem Sci. 2016; 41: 211-8.
32. Hanahan D, Weinberg RA. Hallmarks of cancer: the next generation. Cell. 2011; 144: 646-74.
33. Dang CV. MYC on the path to cancer. Cell. 2012; 149: 22-35.
34. Kroemer G, Pouyssegur J. Tumor cell metabolism: cancer's Achilles' heel. Cancer Cell. 2008; 13: 472-82.
35. Masui K, Tanaka K, Akhavan D et al. mTOR complex 2 controls glycolytic metabolism in glioblastoma through FoxO acetylation and upregulation of c-Myc. Cell Metab. 2013; 18: 726-39.
36. Finley LW, Zhang J, Ye J et al. SnapShot: cancer metabolism pathways. Cell Metab. 2013; 17: 466- e2.
37. Li L, Liang Y, Kang L et al. Transcriptional regulation of the warburg effect in cancer by SIX1. Cancer Cell. 2018; 33(e7): 368-85.
38. Bernstein BE, Hol WG. Crystal structures of substrates and products bound to the phosphoglycerate kinase active site reveal the catalytic mechanism. Biochemistry. 1998; 37: 4429-36.
39. Sun S, Liang X, Zhang X et al. Phosphoglycerate kinase-1 is a predictor of poor survival and a novel prognostic biomarker of chemoresistance to paclitaxel treatment in breast cancer. Br J Cancer. 2015; 112: 1332-9.
40. Hu H, Zhu W, Qin J et al. Acetylation of PGK1 promotes liver cancer cell proliferation and tumorigenesis. Hepatology. 2017; 65: 515-28.
41. Tang SW, Chang WH, Su YC et al. MYC pathway is activated in clear cell renal cell carcinoma and essential for proliferation of clear cell renal cell carcinoma cells. Cancer Lett. 2009; 273: 35-43.
42. Larson SR, Zhang X, Dumpit R et al. Characterization of osteoblastic and osteolytic proteins in prostate cancer bone metastases. Prostate. 2013; 73: 932-40.
43. Yu T, Zhao Y, Hu Z et al. MetaLnc9 facilitates lung cancer metastasis via a PGK1-activated AKT/mTOR pathway. Cancer Res. 2017; 77: 5782-94.
44. Zhang D, Jin N, Sun W et al. Phosphoglycerate mutase 1 promotes cancer cell migration independent of its metabolic activity. Oncogene. 2017; 36: 2900-9.
45. Ren F, Wu H, Lei Y et al. Quantitative proteomics identification of phosphoglycerate mutase 1 as a novel therapeutic target in hepatocellular carcinoma. Mol Cancer. 2010; 9: 81.
46. Sun Q, Li S, Wang Y et al. Phosphoglyceric acid mutase-1 contributes to oncogenic mTOR-mediated tumor growth and confers non-small cell lung cancer patients with poor prognosis. Cell Death Differ. 2018; 25: 1160-73.
47. Gao P, Tchernyshyov I, Chang TC et al. c-Myc suppression of miR-23a/b enhances mitochondrial glutaminase expression and glutamine metabolism. Nature. 2009; 458: 762-5.
48. Xiang S, Gu H, Jin L et al. LncRNA IDH1-AS1 links the functions of c-Myc and HIF1alpha via IDH1 to regulate the Warburg effect. Proc Natl Acad Sci U S A. 2018; 115: E1465-E74.
49. Masson N, Ratcliffe PJ. Hypoxia signaling pathways in cancer metabolism: the importance of co-selecting interconnected physiological pathways. Cancer Metab. 2014; 2: PMID:24491179.
50. Laplante M, Sabatini DM. mTOR signaling in growth control and disease. Cell. 2012; 149: 274-93.
51. Balakirev MY, Tcherniuk SO, Jaquinod M, Chroboczek J. Otubains: a new family of cysteine proteases in the ubiquitin pathway. EMBO Rep. 2003; 4: 517-22.
52. Altun M, Walter TS, Kramer HB et al. The human otubain2-ubiquitin structure provides insights into the cleavage specificity of poly-ubiquitin-linkages. PLoS One. 2015; 10: e0115344.
53. Pan Q, Shai O, Lee LJ et al. Deep surveying of alternative splicing complexity in the human transcriptome by high-throughput sequencing. Nat Genet. 2008; 40: 1413-5.
54. Wang ET, Sandberg R, Luo S et al. Alternative isoform regulation in human tissue transcriptomes. Nature. 2008; 456: 470-6.
55. Yang X, Coulombe-Huntington J, Kang S et al. Widespread expansion of protein interaction capabilities by alternative splicing. Cell. 2016; 164: 805-17.
56. Wang GS, Cooper TA. Splicing in disease: disruption of the splicing code and the decoding machinery. Nat Rev Genet. 2007; 8: 749-61.
57. Jung H, Lee D, Lee J et al. Intron retention is a widespread mechanism of tumor-suppressor inactivation. Nat Genet. 2015; 47: 1242-8.
58. Li X, Qian X, Peng LX et al. A splicing switch from ketohexokinase-C to ketohexokinase-A drives hepatocellular carcinoma formation. Nat Cell Biol. 2016; 18: 561-71.
59. Mackereth CD, Madl T, Bonnal S et al. Multi-domain conformational selection underlies pre-mRNA splicing regulation by U2AF. Nature. 2011; 475: 408-11.
60. Echeverria GV, Cooper TA. Muscleblind-like 1 activates insulin receptor exon 11 inclusion by enhancing U2AF65 binding and splicing of the upstream intron. Nucleic Acids Res. 2014; 42: 1893-903.
61. Yi J, Shen HF, Qiu JS et al. JMJD6 and U2AF65 co-regulate alternative splicing in both JMJD6 enzymatic activity dependent and independent manner. Nucleic Acids Res. 2017; 45: 3503-18.
62. Cho S, Moon H, Loh TJ et al. Splicing inhibition of U2AF65 leads to alternative exon skipping. Proc Natl Acad Sci U S A. 2015; 112: 9926-31.
63. Zhang C, Min L, Zhang L et al. Combined analysis identifies six genes correlated with augmented malignancy from non-small cell to small cell lung cancer. Tumour Biol. 2016; 37: 2193-207.
64. Tian M, Cheng H, Wang Z et al. Phosphoproteomic analysis of the highly-metastatic hepatocellular carcinoma cell line, MHCC97-H. Int J Mol Sci. 2015; 16: 4209-25.
65. Gee MH, Han A, Lofgren SM et al. Antigen Identification for Orphan T Cell Receptors Expressed on Tumor-Infiltrating Lymphocytes. Cell. 2018; 172: 549-63.